

Scaling properties of light-cluster production

Z. Chajęcki,^{1,*} M. Youngs,^{1,2} D.D.S. Coupland,^{1,2} W.G. Lynch,^{1,2,3} M.B. Tsang,^{1,2,3} D. Brown,^{1,2} A. Chbihi,⁴ P. Danielewicz,^{1,2,3} R.T. deSouza,⁵ M.A. Famiano,⁶ T.K. Ghosh,⁷ B. Giacherio,⁶ V. Henzl,¹ D. Henzlova,¹ C. Herlitzius,^{1,3} S. Hudan,⁵ M. A. Kilburn,^{1,2} Jenny Lee,^{1,2} F. Lu,^{3,8} S. Lukyanov,^{1,9} A.M. Rogers,^{1,2} P. Russotto,¹⁰ A. Sanetullaev,^{1,2} R. H. Showalter,^{1,2} L.G. Sobotka,¹¹ Z.Y. Sun,^{1,12} A.M. Vander Molen,¹ G. Verde,¹⁰ M.S. Wallace,^{1,2} and J. Winkelbauer^{1,2}

¹*National Superconducting Cyclotron Laboratory, Michigan State University, East Lansing, MI 48864, USA*

²*Department of Physics and Astronomy, Michigan State University, East Lansing, MI 48864, USA*

³*Joint Institute of Nuclear Astrophysics, Michigan State University, East Lansing, MI 48864, USA*

⁴*GANIL, CEA et IN2P3/CNRS, F-14076 Caen, France*

⁵*Department of Chemistry, Indiana University, Bloomington, IN 47405, USA*

⁶*Department of Physics, Western Michigan University, Kalamazoo, MI 49008, USA*

⁷*Variable Energy Cyclotron Centre, 1/AF Bidhannagar, Kolkata 700064, India*

⁸*Shanghai Institute of Applied Physics, Chinese Academy of Sciences, Shanghai 201800, China*

⁹*FLNR, JINR, 141980 Dubna, Moscow region, Russian Federation*

¹⁰*INFN, Sezione di Catania, I-95123 Catania, Italy*

¹¹*Department of Chemistry, Washington University, St. Louis, MO 63130, USA*

¹²*Institute of Modern Physics, CAS, Lanzhou 730000, Peoples Republic of China*

(Dated: February 24, 2014)

We show that ratios of light-particle energy spectra display scaling properties that can be accurately described by effective local chemical potentials. This demonstrates the equivalence of $t/{}^3\text{He}$ and n/p spectral ratios and provides an essential test of theoretical predictions of isotopically resolved light-particle spectra. In addition, this approach allows direct comparisons of many theoretical n/p spectral ratios to experiments where charged-particle spectra but not neutron spectra are accurately measured. Such experiments may provide much more quantitative constraints on the density and momentum dependence of the symmetry energy.

One of the main uncertainties in the Equation of State (EoS) of neutron-rich nuclear matter concerns the density dependence of the nuclear symmetry energy [1–5]. The symmetry energy increases quadratically with the isospin asymmetry $\delta = (\rho_n - \rho_p)/(\rho_n + \rho_p)$ where ρ_n and ρ_p are the neutron and proton densities, respectively [1–6]. Stable nuclei therefore have small asymmetries. Neutron stars display large asymmetries $\delta \approx 0.8 - 0.9$, driven by the interplay of the Coulomb and symmetry potentials. Accordingly, the density and momentum dependence of the latter strongly influences the internal structure and stability of neutron stars and their temperatures when formed during core-collapse supernovae [5, 7].

Nucleus-nucleus collisions provide the only means to probe the EoS of nuclear matter in the laboratory at densities both below and above saturation density. The symmetry mean-field potential repels neutrons from and attracts protons to a neutron-rich system, leading to predictions that the ratios of neutron (n) over proton (p) center of mass energy spectra provide a sensitive probe of the density and momentum dependence of the symmetry energy [8, 9].

Due to difficulties in precisely knowing neutron detection efficiencies and background corrections, ratios of charged-particle spectra, such as triton (t) over he-

lion (${}^3\text{He}$) spectra, have been proposed as a more accurate surrogate for n/p spectral ratio measurements. The equivalence of $t/{}^3\text{He}$ and n/p spectral ratios, however, has not been experimentally demonstrated until now. Progress requires a better understanding of the production of light clusters.

Many theoretical models directly calculate only the “primordial” nucleon (n and p) spectra prior to cluster formation and do not make direct predictions of bound charged-particle “cluster” spectra [6, 10, 11]. Predictions of light “clusters”, e.g. t or ${}^3\text{He}$ spectra, have been obtained for some models by using the “coalescence” approximation of Butler and Pearson [10, 12], or by using other approximations involving the calculated phase-space densities of nucleons [11, 13, 14] as they decouple from the system. The uncertainties of such approximations strongly influence the accuracy of the symmetry energy information that can be extracted from $t/{}^3\text{He}$ spectral ratios. In many cases more reliable conclusions may be drawn by comparing ratios of measured “coalescence invariant” n and p spectra to corresponding ratios calculated by transport models [2, 15]. Such comparisons are more analogous to comparisons of “primordial” nucleon spectra and are therefore less sensitive to approximations in the theoretical cluster production mechanisms.

In this Letter, we clarify the relationships between spectral ratios by showing that all ratios of light-particle center-of-mass energy spectra can be accurately de-

*Email comments to: chajęcki@nscl.msu.edu

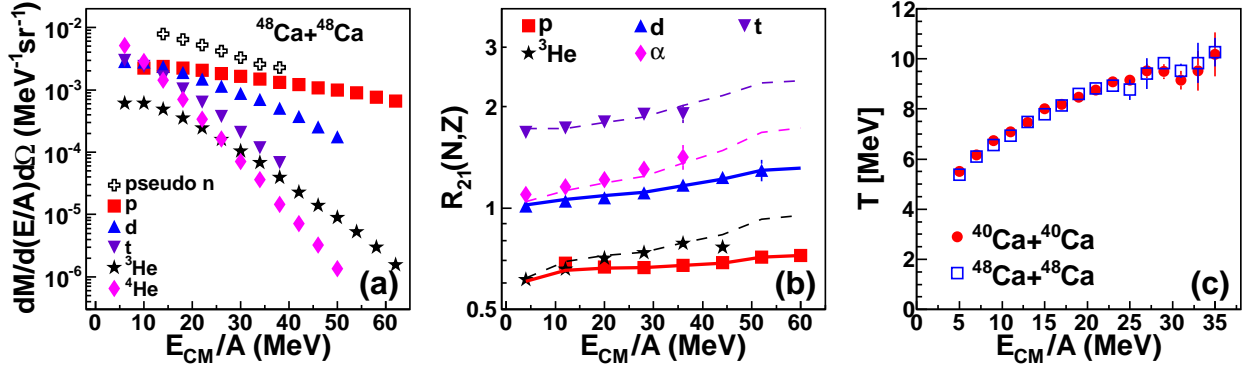


FIG. 1: (Color online) (a) Differential multiplicity distributions for $^{48}\text{Ca}+^{48}\text{Ca}$ collisions at $E/A=80\text{MeV}$, (b) isoscaling yield ratios and (c) the $He-H$ chemical temperature (Eq. 2) from $^{48,40}\text{Ca}+^{48,40}\text{Ca}$ collisions at $E/A = 80\text{ MeV}$. The lines in panel (b) represent the fits using Eq. 1.

scribed by two scaling parameters, related to isoscaling [16], that depend on the velocities of the particles. Some theoretical statistical and dynamical studies relate isoscaling parameters to effective chemical potentials [9, 17, 18]. The present work shows that assuming effective chemical potentials allows more extensive and more powerful comparisons between transport theories and light charged-particle data, facilitating the determination of constraints on the symmetry energy.

We first illustrate these scaling properties by an analysis of experimental measurements of central $^{48}\text{Ca}+^{48}\text{Ca}$ and $^{40}\text{Ca}+^{40}\text{Ca}$ collisions. In the experiment, isotopically enriched ^{48}Ca and ^{40}Ca targets were bombarded with 80 MeV/u ^{48}Ca and ^{40}Ca beams, respectively. Hydrogen (p,d,t) and helium (^3He , α) isotope spectra were measured with the High Resolution Si Strip array (HiRA) [19], which subtended angles of $20^\circ \leq \theta_{\text{LAB}} \leq 60^\circ$, centered about $\theta_{\text{CM}} \approx 90^\circ$. The MSU 4π array [20] was used to select impact parameters with $b < 3\text{ fm}$. Further experimental details can be found in Ref.[21].

Transport calculations predict that the overlap of projectile and target nuclei in central collisions produces a compressed “participant” region whose subsequent expansion reflects the pressure due to the symmetry energy. This pressure can be probed by measurements of energy spectra perpendicular to the beam in the center-of-mass frame, minimizing contributions from the projectile and target residues. The energy spectra for hydrogen and helium isotopes for these systems are found to be nearly independent of the center-of-mass scattering angle in the angular range of $70^\circ < \theta_{\text{CM}} < 110^\circ$. The left panel of Fig. 1 shows energy spectra, $\frac{dM(N,Z)}{dE_{\text{CM}}d\Omega}$ for $^{48}\text{Ca}+^{48}\text{Ca}$, averaged over this angular range to achieve higher statistical precision. All the spectra decrease exponentially with increasing energy. The corresponding spectra for $^{40}\text{Ca}+^{40}\text{Ca}$ display similar trends. These similarities can be easily observed in the middle panel of Fig. 1, where

we show the isoscaling yield ratios

$$R_{21}(N, Z) = \frac{dM_2(N, Z)}{dM_1(N, Z)} = \exp[N\alpha + Z\beta] \quad (1)$$

as a function of E_{CM}/A . In accordance with the isoscaling ratio convention adopted in previous studies [16, 17], system 2 represents the more neutron rich reaction, $^{48}\text{Ca}+^{48}\text{Ca}$, and system 1 represents the neutron deficient reaction, $^{40}\text{Ca}+^{40}\text{Ca}$. The ratios in the middle panel separate into three groups: $R_{21}(t) \approx 1.8$ with $N-Z=1$, $R_{21}(d) \approx R_{21}(\alpha) \approx 1.1$ with $N=Z$, and $R_{21}(p) \approx R_{21}(^3\text{He}) \approx 0.7$ with $N-Z=-1$. Each ratio increases gradually as a function of energy and this grouping becomes less distinct with increasing E_{CM}/A .

In a number of statistical and dynamical models [16–18, 22–24], the isoscaling parameters α and β can be related to the differences in *effective* neutron and proton chemical potentials, μ_n and μ_p , between reactions 2 and 1, as well as the effective chemical temperature T . In such cases, $\alpha = \Delta\mu_n/T$ and $\beta = \Delta\mu_p/T$ and $\Delta\mu_n = (\mu_{n,2} - \mu_{n,1})$, $\Delta\mu_p = (\mu_{p,2} - \mu_{p,1})$. These expressions assume that the effective temperature T is the same in both systems 1 and 2. To examine this assumption, we use the $p, d, ^3\text{He}$ and α spectra to construct the $He-H$ chemical temperature, which assumes chemical equilibrium at freezeout [25–28]:

$$T = \frac{14.3}{\log[1.59R_{He-H}]}, \quad (2)$$

where $R_{He-H} = \frac{dM_d/d\Omega dE \cdot dM_{^3\text{He}}/d\Omega dE}{dM_t/d\Omega dE \cdot dM_\alpha/d\Omega dE}$. The sensitivity of the $He-H$ thermometer to T stems from the large, 21.6 MeV, binding energy difference between α and ^3He clusters, which favors α relative to ^3He production at low temperature. The right panel of Fig. 1 shows that the extracted $He-H$ isotope temperature values at $\theta_{\text{CM}} \approx 90^\circ$ for $^{40}\text{Ca}+^{40}\text{Ca}$ collisions (full red circles) and $^{48}\text{Ca}+^{48}\text{Ca}$ collisions (open blue squares) are indistinguishable, which can be expected for equal center-of-mass

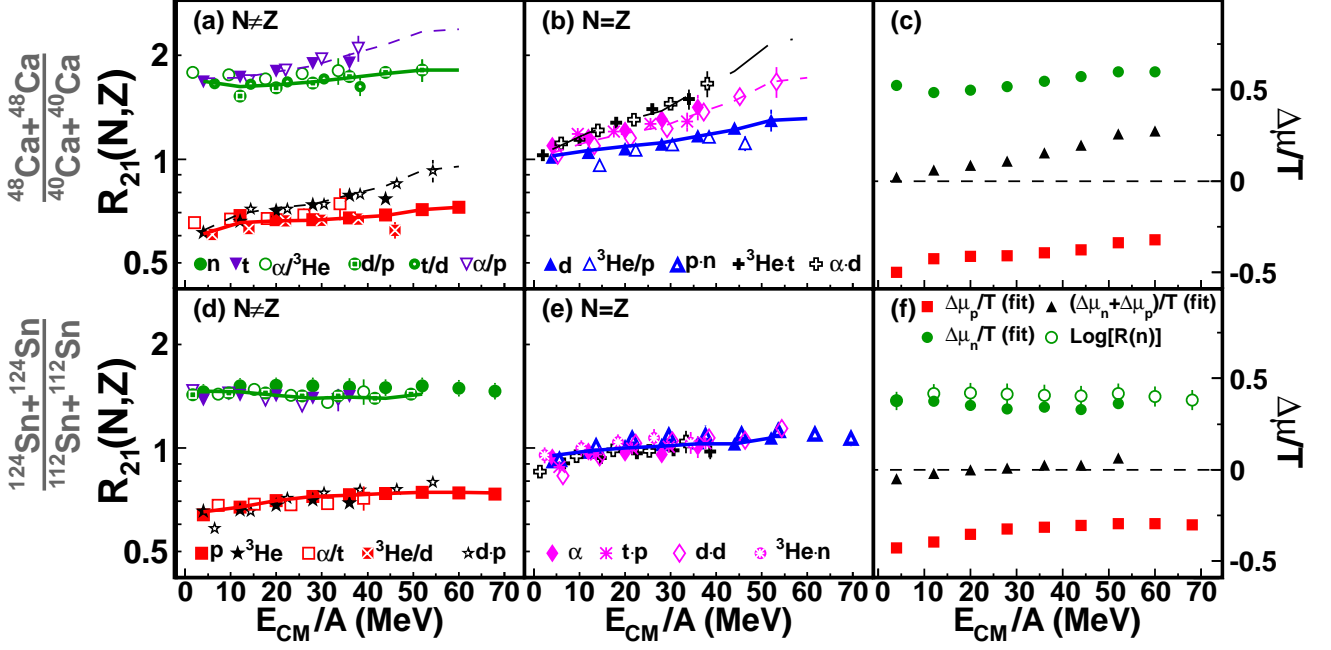


FIG. 2: (Color online) Isoscaling yield ratios as well as their combinations for (a) and (d) $N \neq Z$ fragments, (b) and (e) $N = Z$ fragments, (c) and (f) overall fit results (solid symbols) using Eq. 1. The data points representing the combinations of isoscaling yield ratios in panels (a),(b), (d) and (e) were slightly offset with respect to their average values of E_{CM}/A to improve the readability of the figure. The open symbols in (f) represent the values calculated from the measured neutron ratios. The lines in (a),(b),(d) and (e) represent the fit results using Eq. 1. The neutron ratio and the combinations of ratios that involve neutrons were not included in the fit, consistent with the treatment for Ca+Ca reactions. The top and bottom panels show results from the $^{48,40}\text{Ca} + ^{48,40}\text{Ca}$ and $^{124,112}\text{Sn} + ^{124,112}\text{Sn}$ collisions, respectively.

kinetic energies per nucleon for these two systems [29]. The monotonic decrease of T with decreasing E_{CM}/A reflects the cooling of the participant source at later stages of the expansion.

The divergent trends of each isotope in the middle panel of Fig. 1 can be described accurately by two isoscaling parameters α and β , which both depend on the E_{CM}/A of the outgoing particle. Accordingly, fits to $R_{21}(p)$, $R_{21}(t)$, $R_{21}(^3\text{He})$ and $R_{21}(\alpha)$ are shown as the lines in middle panel of Fig. 1. These fits agree very well with the data. This agreement implies fundamental equalities such as $R_{21}(N_1 + N_2, Z_1 + Z_2) = R_{21}(N_1, Z_1) \cdot R_{21}(N_2, Z_2)$ and $R_{21}(N_1 - N_2, Z_1 - Z_2) = R_{21}(N_1, Z_1)/R_{21}(N_2, Z_2)$ between $R_{21}(N, Z)$ values for the various isotopes. For example, it predicts that $R_{21}(n) = R_{21}(d)/R_{21}(p) = R_{21}(t)/R_{21}(d)$, which is a breakthrough that could obviate part of the need to measure neutrons, and facilitate more quantitative comparisons between measured and calculated charged particle spectra.

From the measured spectra of $p, d, t, ^3\text{He}$ and alpha particles, we can test the consistency of n-like ratios with $N-Z=1$: $R_{21}(n)$, $R_{21}(t)$, $R_{21}(\alpha)/R_{21}(^3\text{He})$, $R_{21}(d)/R_{21}(p)$, $R_{21}(t)/R_{21}(d)$, $R_{21}(\alpha)/R_{21}(p)$, and p-like ratios with $N-Z=-1$: $R_{21}(p)$, $R_{21}(^3\text{He})$, $R_{21}(^3\text{He})/R_{21}(d)$,

$R_{21}(d)R_{21}(p)$ and $R_{21}(\alpha)/R_{21}(t)$ which are shown in the left top panels of Fig. 2. We also construct the deuteron-like ratios with $N=Z$: $R_{21}(d)$, $R_{21}(\alpha)$, $R_{21}(p)R_{21}(n)$, $R_{21}(^3\text{He})/R_{21}(p)$, $R_{21}(^3\text{He})R_{21}(t)$, $R_{21}(\alpha)R_{21}(d)$, $R_{21}(t)R_{21}(p)$, $R_{21}(d)R_{21}(d)$, $R_{21}(^3\text{He})R_{21}(n)$ as shown in Fig. 2 (b). The isoscaling parameters $\alpha = \Delta\mu_n/T$ and $\beta = \Delta\mu_p/T$ shown in Fig. 2(c) were determined from the fits to all the distributions presented in Fig. 2(a) and (b) using Eq. 1.

To test the applicability of such analyses to predict energy spectra of neutrons, which were not measured in Ca+Ca experiment, we next investigate n , p , d , t , ^3He and ^4He energy spectra measured for central $^{112}\text{Sn} + ^{112}\text{Sn}$ and $^{124}\text{Sn} + ^{124}\text{Sn}$ collisions at $E/A=50$ MeV from another experiment at the Coupled Cyclotron Facility (CCF) at Michigan State University [30]. In this experiment, we selected central collisions, $b < 3fm$ by measuring the charged-particle multiplicity and transverse energy using the MSU Miniball Array[31]. Spectra for hydrogen and helium isotopes were measured with 6 telescopes of the Large Area Silicon Strip Array (LASSA) [32] and neutrons were measured with the Large Area Neutron Array (LANA) [33]. Further experimental details can be found in Ref. [30].

The left panel of Fig. 3 shows the energy spectra,

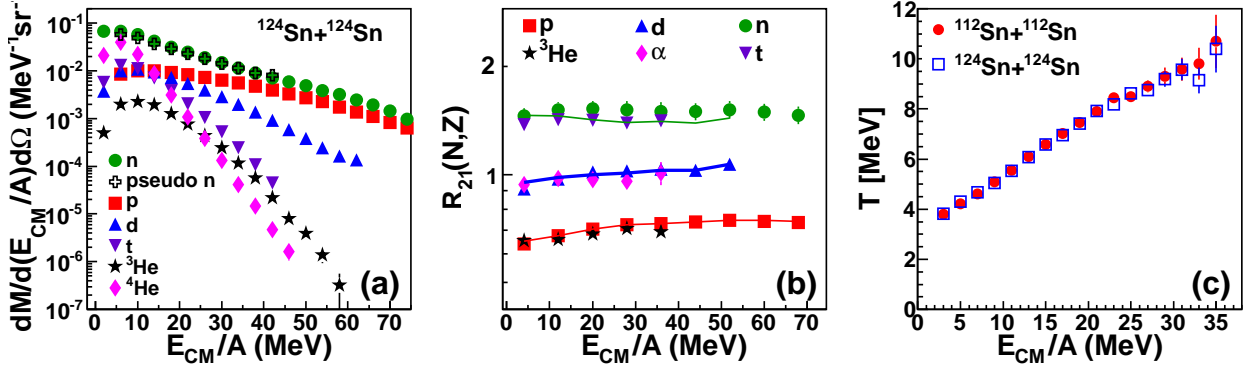


FIG. 3: (Color online) (a) Differential multiplicity distributions for $^{124}\text{Sn}+^{124}\text{Sn}$ collisions at $E/A=50\text{ MeV}$, (b) isoscaling yield ratios and (c) the $He-H$ chemical temperature (Eq. 2) from $^{124,112}\text{Sn}+^{124,112}\text{Sn}$ collisions at $E/A=50\text{ MeV}$. The lines in panel (b) represent the fits using Eq. 1.

$\frac{dM(N,Z)}{dE_{CM}d\Omega}$, measured for $^{124}\text{Sn}+^{124}\text{Sn}$ collisions, and the right panel of Fig. 3 shows the corresponding equivalence of temperature values for $^{112}\text{Sn}+^{112}\text{Sn}$ collisions (full red circles) and $^{124}\text{Sn}+^{124}\text{Sn}$ collisions (open blue squares). The middle panel of Fig. 3 shows the ratios $R_{21}(N,Z)$ (Eq. 1) of the energy spectra for $^{124}\text{Sn}+^{124}\text{Sn}$ collisions divided by those for $^{112}\text{Sn}+^{112}\text{Sn}$ collisions. Similar to Ca+Ca systems, the Sn+Sn ratios vary gradually with energy and separate into three groups: $R_{21}(n) \approx R_{21}(t) \approx 1.5$ with $N-Z=1$, $R_{21}(d) \approx R_{21}(\alpha) \approx 1$ with $N=Z$, and $R_{21}(p) \approx R_{21}(^3\text{He}) \approx 0.7$ with $N-Z=-1$. Unlike Ca+Ca, however, $R_{21}(d) \approx R_{21}(\alpha)$ and the various ratios constructed from the measured fragments for Sn+Sn follow the trends of $R_{21}(n)$, $R_{21}(d)$ and $R_{21}(p)$ more closely; see Figs. 2(d) and (e). Consistent with this observation, the fit parameters $\alpha = \Delta\mu_n/T$ and $\beta = \Delta\mu_p/T$ in Fig. 2(f) satisfy $(\alpha + \beta) \approx 0$ for these Sn+Sn collisions. The identities $R_{21}(p) = R_{21}(^4\text{He})/R_{21}(t) = R_{21}(^3\text{He})/R_{21}(d)$ and $R_{21}(n) = R_{21}(d)/R_{21}(p) = R_{21}(t)/R_{21}(d)$ apply to Sn+Sn collisions in Fig. 2 (d)-(e) as well as they do to Ca+Ca collisions in Fig. 2(a)-(b). These scaling behaviors indicate that light-particle emission can be well described by local chemical equilibrium.

To successfully extract symmetry energy constraints directly from isotopically resolved energy spectra, theories should replicate these scaling properties and reproduce the abundances of isoscalar α and d particles at the E_{CM}/A values of interest, since the yields of such isoscalar particles correlate positively with the n/p and $t/^3\text{He}$ ratios due to the constraints of charge and baryon number conservation [34, 35]. If theories fail these tests, comparisons can nevertheless be made between theoretical and experimental “coalescence invariant” primordial neutron and proton spectra constructed by combining free nucleons with those bound in clusters. This requires both isotopically resolved charged-particle and free neutron spectra, but few experiments measure neutrons.

To address the lack of neutron data for central heavy

ion collisions, one can use chemical potential scaling to provide relatively accurate estimates for neutron spectra. Applying chemical potential scaling to ratios of spectra within the same isospin multiplet and in the same reaction, chemical potential scaling predicts that the product of the measured triton over helion spectra times the measured proton spectra provides a “pseudo” neutron spectrum, i.e. $\frac{dM(n)_{pseudo}}{dE} = \frac{dM(p)}{dE} \cdot \frac{dM(2,1)}{dM(1,2)}$. A somewhat similar procedure has also been proposed in Ref. [36]. The open black crosses in Fig. 1(a) and 3(a) show “pseudo” neutron spectra for the $^{48}\text{Ca}+^{48}\text{Ca}$ and $^{124}\text{Sn}+^{124}\text{Sn}$ reaction respectively. We compare “pseudo” (open black crosses) and free neutron (green circles) spectra in Fig. 3(a); these two spectra agree to within 10% for $E_{CM}/A > 20\text{ MeV}$. Larger discrepancies might be expected at low energies, due to the Coulomb repulsion from the residue and the difference between the charges for the n , p , t and ^3He ejectiles. However, significantly large residues do not survive in central Sn+Sn collisions at $E/A=50\text{ MeV}$, reducing such effects [37, 38]. Free or pseudo neutron spectra provide the large contributions to the coalescence invariant neutron spectra at $E_{CM}/A > 20\text{ MeV}$, but not at lower energies where more neutrons are directly observed in clusters, reducing uncertainties due to Coulomb effects. For such reactions where neutrons have not been measured, pseudo-neutron spectra can allow more quantitative constraints on the momentum dependence of the symmetry energy to be extracted, accelerating progress in this important area.

When local chemical equilibrium is achieved, models predict the effective chemical potential scaling parameters to contain relevant information about the symmetry mean field potentials. For example, statistical expressions for these scaling parameters $\alpha = \Delta\mu_n/T$ and $\beta = \Delta\mu_p/T$ can be found in Ref. [17]. In the Expanding Evaporation Source model (EES), for example, α depends on the neutron separation energy, the excitation energy and entropy per neutron, and β depends on the corresponding proton properties [17]. The separation en-

ergies clearly depend on the density and momentum dependence of the symmetry energy within the source, and the entropies and excitation energies are strongly dependent on its momentum dependence. In the environment of a collision like the ones investigated here, transport theory predicts these sensitivities to the symmetry energy to remain, but the sensitivity to the momentum dependence also reflects the non-thermal relative nucleonic velocities that requires transport theory for this description [8, 39].

In summary, we have shown that the energy spectra of nucleons and light bound nuclei follow scaling laws related to isoscaling and to local chemical potentials. This provides an important test of transport theory and confirms the equivalence of n/p to $t/{}^3\text{He}$ spectral ratios for systems that totally disintegrate reducing the differences between Coulomb barriers for such particles. We discuss the importance of avoiding the limitations of the cluster production mechanisms of certain models by constructing coalescence invariant primordial neutron and proton spectra. Such spectra are less sensitive to the final state interactions that produce the clusters observed in experiment. We have successfully applied chemical potential scaling to individual reactions to accurately predict the neutron spectra. This will expand considerably the systems from which constraints on the symmetry energy can be obtained accelerating progress in this area.

This work is supported by Michigan State University, the Joint Institute for Nuclear Astrophysics, the National Science Foundation Grants No. PHY-0216783, PHY-1102511, PHY-1068571, PHY-0822648, and PHY-0855013, and the U.S. Department of Energy Division of Nuclear Physics Grant No. DE-FG02-87ER-40316 and Contract No. DE-AC02-06CH11357.

[1] A. W. Steiner, M. Prakash, J. M. Lattimer, and P. J. Ellis, *Phys.Rept.* **411**, 325 (2005).
 [2] P. Danielewicz, R. Lacey, and W. G. Lynch, *Science* **298**, 1592 (2002).
 [3] M. B. Tsang, Y. Zhang, P. Danielewicz, M. Famiano, Z. Li, et al., *Phys.Rev.Lett.* **102**, 122701 (2009).
 [4] M. B. Tsang, J. Stone, F. Camera, P. Danielewicz, S. Gandolfi, et al., *Phys.Rev.* **C86**, 015803 (2012).
 [5] J. Lattimer and M. Prakash, *Astrophys.J.* **550**, 426 (2001).
 [6] B.-A. Li, L.-W. Chen, and C. M. Ko, *Phys.Rept.* **464**, 113 (2008).
 [7] J. Pons, S. Reddy, M. Prakash, J. Lattimer, and J. Miralles, *Astrophys.J.* **513**, 780 (1999).
 [8] J. Rizzo, M. Colonna, and M. Di Toro, *Phys.Rev.* **C72**, 064609 (2005).
 [9] M. Di Toro, V. Baran, M. Colonna, and V. Greco, *J.Phys.* **G37**, 083101 (2010).
 [10] P. Danielewicz and G. F. Bertsch, *Nucl.Phys.* **A533**, 712

(1991).
 [11] L.-W. Chen, C. M. Ko, and B.-A. Li, *Phys.Rev.* **C68**, 017601 (2003).
 [12] S. T. Butler and C. A. Pearson, *Phys.Rev.* **129**, 836 (1963).
 [13] J. Aichelin, *Phys.Rept.* **202**, 233 (1991).
 [14] M. Colonna, A. Ono, and J. Rizzo, *Phys.Rev.* **C82**, 054613 (2010).
 [15] M. Famiano, T. Liu, W. Lynch, A. Rogers, M. Tsang, et al., *Phys.Rev.Lett.* **97**, 052701 (2006).
 [16] M. Tsang, W. Friedman, C. Gelbke, W. Lynch, G. Verde, et al., *Phys.Rev.Lett.* **86**, 5023 (2001).
 [17] M. B. Tsang, C. K. Gelbke, X. D. Liu, W. G. Lynch, W. P. Tan, et al., *Phys.Rev.* **C64**, 054615 (2001).
 [18] A. Ono, P. Danielewicz, W. A. Friedman, W. G. Lynch, and M. B. Tsang, *Phys.Rev.* **C68**, 051601 (2003).
 [19] M. S. Wallace, M. A. Famiano, M. J. van Goethem, A. M. Rogers, W. G. Lynch, J. Clifford, F. Delaunay, J. Lee, S. Labostov, M. Mocko, et al., *Nucl. Instr. and Meth. A* **583**, 302 (2007).
 [20] G. D. Westfall et al., *Nucl. Instrum. Meth.* **A238**, 347 (1985).
 [21] V. Henzl, M. A. Kilburn, Z. Chajecski, D. Henzlova, W. G. Lynch, et al., *Phys.Rev.* **C85**, 014606 (2012).
 [22] S. Das Gupta and A. Z. Mekjian, *Phys.Rept.* **72**, 131 (1981).
 [23] G. Fai and A. Z. Mekjian, *Phys.Lett.* **B196**, 281 (1987).
 [24] A. S. Botvina, O. V. Lozhkin, and W. Trautmann, *Phys.Rev.* **C65**, 044610 (2002).
 [25] H. Xi, W. G. Lynch, M. B. Tsang, and W. A. Friedman, *Phys.Rev.* **C54**, R2163 (1996).
 [26] M. B. Tsang, W. G. Lynch, H. Xi, and W. A. Friedman, *Phys.Rev.Lett.* **78**, 3836 (1997).
 [27] S. Albergo, S. Costa, E. Costanzo, and A. Rubbino, *Nuovo Cim.* **A89**, 1 (1985).
 [28] J. Natowitz, R. Wada, K. Hagel, T. Keutgen, M. Murray, et al., *Phys.Rev.* **C65**, 034618 (2002).
 [29] G. Kunde, S. Gaff, C. Gelbke, T. Glasmacher, M. Huang, R. Lemmon, W. Lynch, L. Manduci, L. Martin, M. Tsang, et al., *Physics Letters B* **416**, 56 (1998).
 [30] D. Coupland et al., in preparation (2013).
 [31] R. T. De Souza, N. Carlin, Y. D. Kim, J. Ottarson, L. Phair, et al., *Nucl.Instrum.Meth.* **A295**, 109 (1990).
 [32] B. Davin, R. T. de Souza, R. Yanez, Y. Larochele, R. Alfaro, H. S. Xu, A. Alexander, K. Bastin, L. Beaulieu, J. Dorsett, et al., *Nucl. Instr. and Meth. A* **473**, 302 (2001).
 [33] J. K. P.D Zecher, A Galonsky et al., *Nucl. Instr. and Meth. A* **401**, 329 (1997).
 [34] L. Shi and P. Danielewicz, *Europhys.Lett.* **49**, 34 (2000).
 [35] L. G. Sobotka, J. F. Dempsey, R. J. Charity, and P. Danielewicz, *Phys.Rev.* **C55**, 2109 (1997).
 [36] K. Hagel, R. Wada, J. Cibor, M. Lunardon, N. Marie, et al., *Phys.Rev.* **C62**, 034607 (2000).
 [37] S. Hudan et al. (INDRA Collaboration), *Phys.Rev.* **C67**, 064613 (2003).
 [38] T. Liu, W. Lynch, M. Tsang, X. Liu, R. Shomin, et al., *Phys.Rev.* **C76**, 034603 (2007).
 [39] C. B. Das, S. Das Gupta, C. Gale, and B.-A. Li, *Phys.Rev.* **C67**, 034611 (2003).